Monthly Notices
of the
ROYAL ASTRONOMICAL SOCIETY

MNRAS **463,** 4311–4316 (2016)
Advance Access publication 2016 September 9

doi:10.1093/mnras/stw2278

Standardizing Type Ia supernovae optical brightness using near-infrared rebrightening time

H. Shariff,[1,2]★ S. Dhawan,[3,4,5] X. Jiao,[2,6] B. Leibundgut,[3,4] R. Trotta[1,2,6]★ and D. A. van Dyk[2,6,7]

[1]*Physics Department, Astrophysics Group, Imperial College London, Prince Consort Rd, London SW7 2AZ, UK*
[2]*Imperial Centre for Inference and Cosmology, Blackett Laboratory, Prince Consort Rd, London SW7 2AZ, UK*
[3]*European Southern Observatory, Karl-Schwarzschild-Strasse 2, D-85748 Garching bei München, Germany*
[4]*Excellence Cluster Universe, Technische Universität München, Boltzmannstrasse 2, D-85748 Garching, Germany*
[5]*Physik Department, Technische Universität München, James-Franck-Strasse 1, D-85748 Garching bei München, Germany*
[6]*Data Science Institute, William Penney Laboratory, Imperial College London, London SW7 2AZ, UK*
[7]*Mathematics Department, Statistics Section, Huxley Building, Imperial College London, London SW7 2AZ, UK*

Accepted 2016 September 8. Received 2016 August 22; in original form 2016 June 20

ABSTRACT

Accurate standardization of Type Ia supernovae (SNIa) is instrumental to the usage of SNIa as distance indicators. We analyse a homogeneous sample of 22 low-z SNIa, observed by the Carnegie Supernova Project in the optical and near-infrared (NIR). We study the time of the second peak in the J band, t_2, as an alternative standardization parameter of SNIa peak optical brightness, as measured by the standard *SALT2* parameter m_B. We use *BAHAMAS*, a Bayesian hierarchical model for SNIa cosmology, to estimate the residual scatter in the Hubble diagram. We find that in the absence of a colour correction, t_2 is a better standardization parameter compared to stretch: t_2 has a 1σ posterior interval for the Hubble residual scatter of $\sigma_{\Delta\mu} = \{0.250, 0.257\}$ mag, compared to $\sigma_{\Delta\mu} = \{0.280, 0.287\}$ mag when stretch (x_1) alone is used. We demonstrate that when employed together with a colour correction, t_2 and stretch lead to similar residual scatter. Using colour, stretch and t_2 jointly as standardization parameters does not result in any further reduction in scatter, suggesting that t_2 carries redundant information with respect to stretch and colour. With a much larger SNIa NIR sample at higher redshift in the future, t_2 could be a useful quantity to perform robustness checks of the standardization procedure.

Key words: methods: data analysis – methods: statistical – supernovae: general – distance scale.

1 INTRODUCTION

Type Ia supernovae (SNIa) are exceptionally useful distance indicators in cosmology and have been instrumental in the discovery of the accelerated expansion of the Universe (Riess et al. 1998; Perlmutter et al. 1999). Their apparent magnitudes must be 'standardized' by correcting for empirical correlations between observable properties and intrinsic magnitude in order to reduce residual scatter sufficiently to measure cosmological parameters (Phillips 1993; Riess, Press & Kirshner 1996; Tripp 1998).

To date, cosmological parameter constraints from SNIa have been derived from optical light-curve data. There are, however, clear indications that near-infrared (NIR) data improve precision and accuracy further (Mandel, Narayan & Kirshner 2011). At NIR wavelengths (900 nm $< \lambda <$ 2400 nm), SNIa exhibit more uniform brightness, without the need for empirical standardization (Krisciunas, Phillips & Suntzeff 2004; Wood-Vasey et al. 2008; Mandel et al. 2009; Mandel, Narayan & Kirshner 2011). The scatter in the peak luminosity in these studies can be as low as 0.1 mag. Furthermore, NIR light is less affected by extinction due to dust, which makes NIR data less prone to pernicious dust-related systematics. Distances in the NIR can be measured to better than 6 per cent precision, making this wavelength region an exciting prospect for SNIa cosmology (Kattner et al. 2012).

The light-curve morphology in the NIR is markedly different from that in the optical, showing a pronounced second maximum in *IYJHK* filters for 'normal' SNIa (Elias et al. 1981; Leibundgut 1988; Hamuy et al. 1996; Folatelli et al. 2010). This rebrightening offers interesting clues into the physics of the explosion. The timing of the second maximum (t_2, measured as the time between B-band maximum light and the second maximum in a given NIR filter) in the *YJHK* filters is strongly correlated with the optical decline rate

★ E-mail: hikmatali.shariff11@imperial.ac.uk (HS); r.trotta@imperial.ac.uk (RT)

of SNIa (measured by the Δm_{15} parameter) as shown in Biscardi et al. (2012) and Dhawan et al. (2015). Kasen (2006), based on radiative transfer calculations of synthetic light curves, predicted that t_2 is a function of the ^{56}Ni mass produced by the SNIa. Indeed, Dhawan et al. (2016) found a strong correlation between the peak bolometric luminosity (and therefore, ^{56}Ni mass; see Arnett 1982) and t_2 for a sample of SNIa with low extinction from host galaxy dust. They demonstrate that this parameter can be used to infer the ^{56}Ni mass for SNIa.

There are many reasons why t_2 is a potentially useful quantity for SNIa cosmology. First, since t_2 is a timing (and not a flux) estimate, it is unaffected by host galaxy reddening, which is not the case for optical decline rate parameters, e.g. x_1 and Δm_{15} (see Amanullah & Goobar 2011, for a discussion). Secondly, the rebrightening in the NIR is due to an ionization transition of Fe-group elements from doubly to singly ionized atoms at a transition temperature ∼7000 K (see Kasen 2006; Blondin, Dessart & Hillier 2015). The time at which this transition occurs is driven by the amount of heating from ^{56}Ni produced by the explosion. Since ^{56}Ni is the primary energy source for the peak brightness of the SNIa (Arnett 1982), t_2 would be expected to correlate strongly with the peak magnitude of the SNIa and hence be an effective parameter for standardization.

Thirdly, the rebrightening in the NIR is an exclusive feature of SNIa, not observed in any other type of SN. This makes the second maximum a useful indicator to distinguish SNIa from other types of SNe in absence of spectroscopic confirmation. Therefore, observing the NIR second maximum could become critical for photometric classification of SNIa in future SN surveys. Given that such data should become available with future facilities – e.g. *Euclid* (expected launch 2019), *JWST* (expected 2018), *Wide-Field Infrared Survey Telescope* (*WFIRST*, expected launch ∼ 2020; see Hook 2013, for a review) – studying the standardization properties of t_2 can provide an alternative and more robust route to SNIa cosmology at no additional observational cost. Furthermore, the time-delay between the optical peak brightness and NIR rebrightening means that NIR observations can be scheduled without the need for prompt alerts required to sample densely the optical light curve near its peak, which is necessary for an accurate estimate of Δm_{15}.

The aim of this work is to compare the residual scatter in magnitudes after empirical standardization for a sample of nearby SNIa using the traditional stretch parameter (x_1) versus what can be obtained when using t_2 instead (or in addition). We address the question of whether the NIR rebrightening time can be used to reduce the residual scatter in the peak luminosity of SNIa. This paper is structured as follows. In Section 2, we describe the data set we use and present the Bayesian methodology for our analysis including a description of the parameters of interest. We present the results of applying our method to this low-z SNIa data set in Section 3 and conclude in Section 4.

2 METHODOLOGY

2.1 Data

We have compiled a sample of 22 SNIa, in the redshift range $0.01 \leq z \leq 0.047$, all with well-sampled optical and NIR photometry. In this paper, we only make use of J-band NIR data. The source of NIR SNIa photometry is the Carnegie Supernova Project (CSP; Contreras et al. 2010; Stritzinger et al. 2011). The low-z CSP provides a sample of SNIa with optical and NIR light curves in a homogeneous and well-defined photometric system (the Vega magnitude system) and thus forms an ideal base for the evaluation of light-curve properties.

The *SALT2* fit parameters, i.e. peak B-band magnitude m_B, light-curve stretch correction x_1, and colour correction c, (Guy et al. 2007) are taken from the analysis in Rest et al. (2014). The total number of SNIa with J-band t_2 estimates is larger than presented here, however, we only use the subset analysed as part of the low-z anchor in Rest et al. (2014). The NIR rebrightening time, t_2, in the J band, is evaluated as described in Dhawan et al. (2015) and subsequently re-centred to the sample mean value, $\langle t_2 \rangle = 27.96$ d.

2.2 Setup and method

In order to determine the standardization parameters and residual dispersion in the SNIa magnitudes, we use the Bayesian hierarchical method *BAHAMAS* (Shariff et al. 2016). March et al. (2011) introduced Bayesian hierarchical modelling to the problem of cosmological parameter extraction from *SALT2* fits. The key feature is the hierarchical treatment of sources of uncertainty, comprising of both measurement errors and population variability. Each observed covariate (for example, $\hat{m}_{Bi}$, the observed apparent magnitude of the ith SNIa) is assumed to have an underlying true (latent) value (for example, m_{Bi}, the real apparent magnitude of the ith SNIa) that is unobserved. Linear regression is then applied to the true value of the covariate, which itself is drawn probabilistically from a distribution describing the population of SNIa. Finally, latent values are marginalized from the posterior distribution. Shariff et al. (2016) further developed this Bayesian approach to include additional (or alternative) covariates for the standardization of SNIa, and to provide explicit sampling of the latent variables. We refer to Shariff et al. (2016) for full details about the hierarchical model and the sampling methods (see also Nielsen, Guffanti & Sarkar 2015 for a similar model but applied under a frequentist framework; see Rubin et al. 2015 for a different implementation of a similar hierarchical Bayesian model, and Ma, Corasaniti & Bassett 2016 for an analysis using Bayesian graphs).

Another feature that distinguishes this Bayesian procedure from the standard χ^2 approach is the treatment of the absolute magnitude of SNIas. Rather than assuming that all SNIas have the same intrinsic magnitude (and then inflate the observational errors to obtain $\chi^2/\mathrm{dof} = 1$, as in the standard approach), each SNIa, after applying empirical corrections, has its own residual absolute magnitude, M_i^ϵ. These are assumed to follow an underlying Gaussian distribution (denoted by $\mathcal{N}$), $M_i^\epsilon \sim \mathcal{N}(M_0, \sigma_{\rm res}^2)$, whose mean, M_0, and residual dispersion, $\sigma_{\rm res}$, are determined from the data. Similarly, the other latent parameters are modelled hierarchically as $x_{1i} \sim \mathcal{N}(x_{1\star}, R_{x_1}^2)$, $t_{2i} \sim \mathcal{N}(t_{2\star}, R_{t_2}^2)$ and $c_i \sim \mathcal{N}(c_\star, R_c^2)$, i.e. the aforementioned distributions describing the population of SNIa, where the means and standard deviations of the distributions are Bayesianly determined from the data.

This hierarchical structure has an advantage of 'borrowing strength', in particular, when estimating the scatter of the SNIa absolute magnitudes that is not predicted by the covariates ($\sigma_{\rm res}$). March et al. (2011) also showed that this method reduces the mean squared error of the parameter estimators when compared to the standard approach. In this work, we extend *BAHAMAS* to include t_2 as an additional linear covariate (or as an alternative to x_1). A full treatment of optical and infrared light-curve data in terms of a Bayesian hierarchical methodology is presented in Mandel et al. (2009). Also, Kim et al. (2013) use Gaussian Process regression to perform a non-parametric fit to spectrophotometric time series from the Nearby Supernova Factory.

Table 1. Summary of the parameters, notations, and prior distributions used in our hierarchical model. 'SD' stands for 'standard deviation'. See Shariff et al. (2016) for more details.

Parameter	Notation and prior distribution
Covariates	
Negative of the coefficient of stretch covariate	$\alpha \sim \text{Uniform}(-1, 1)$
Coefficient of colour covariate	$\beta \sim \text{Uniform}(-4, 4)$
Negative of the coefficient of NIR rebrightening time	$\gamma \sim \text{Uniform}(-1, 1)$
Population-level distributions	
Mean of absolute magnitudes	$M_0^{\epsilon} \sim \mathcal{N}(-19.3, 2^2)$
Residual scatter after corrections	$\sigma_{\text{res}}^2 \sim \text{InvGamma}(0.003, 0.003)$
Mean of stretch	$x_{1\star} \sim \mathcal{N}(0, 10^2)$
SD of stretch	$R_{x_1} \sim \text{LogUniform}(-5, 2)$
Mean of t_2	$t_{2\star} \sim \mathcal{N}(0, 10^2)$
SD of t_2	$R_{t_2} \sim \text{LogUniform}(-5, 2)$
Mean of colour	$c_\star \sim \mathcal{N}(0, 1^2)$
SD of colour	$R_c \sim \text{LogUniform}(-5, 2)$

The generalized Phillips corrections, including any number of (linear) covariates can be written as

$$m^{\star}_{Bi} = \mu_i(\hat{z}_i, \mathscr{C}) + X_i^T \mathscr{B} + M_i^{\epsilon}, \tag{1}$$

where $\mu_i(\hat{z}_i, \mathscr{C})$ is the distance modulus at the observed redshift $\hat{z}_i$ for cosmological parameters $\mathscr{C}$, X_i is a vector of covariates, and $\mathscr{B}$ is the vector of regression coefficients. In the standard *SALT2* analysis, $X_i = \{x_{1i}, c_i\}$ and $\mathscr{B} = \{-\alpha, \beta\}$, where α is the slope of the stretch correction parameter and β is the slope of the colour correction parameter. In this analysis, we consider five cases.

(i) $X_i = \{x_{1i}\}$ and $\mathscr{B} = \{-\alpha\}$
(ii) $X_i = \{t_{2i}\}$ and $\mathscr{B} = \{-\gamma\}$
(iii) $X_i = \{x_{1i}, c_i\}$ and $\mathscr{B} = \{-\alpha, \beta\}$
(iv) $X_i = \{t_{2i}, c_i\}$ and $\mathscr{B} = \{-\gamma, \beta\}$
(v) $X_i = \{x_{1i}, t_{2i}, c_i\}$ and $\mathscr{B} = \{-\alpha, -\gamma, \beta\}$,

where γ is the NIR rebrightening parameter, giving the (negative of the) slope of the linear relationship between t_2 and intrinsic magnitude (so a larger value of t_2 corresponds to brighter objects).

We adopt a flat Λcold dark matter cosmology with fixed cosmological parameters, $\mathscr{C} = \{\Omega_{\text{m}} = 0.3, w = -1, H_0 = 70\}$, where Ω_{m} is the matter density parameter, w the dark energy equation of state parameter, and H_0 the Hubble parameter today (in $\text{km}^{-1}\text{s}^{-1}\text{Mpc}^{-1}$). We fix the cosmology since these parameters are unconstrained by SNIa data alone: in the redshift range covered by our SNIa data, the luminosity distance is essentially linear with redshift, with the slope of the relationship given by c/H_0, with c being the speed of light. The adopted value of H_0 is completely degenerate with the average intrinsic magnitude of the SNIas, M_0.

The priors for the other parameters in our model are given in Table 1. A significant fraction of the residual dispersion in low-z SNIa is due to peculiar velocities, since these objects are not fully in the Hubble flow. To account for the variance due to peculiar velocities, we follow a procedure similar to Mandel et al. (2009). Specifically, we add a term, σ_μ^2, to the apparent magnitude error; σ_μ^2 depends on the peculiar velocities uncertainty, σ_{pec}, and redshift measurement error, σ_z, as

$$\sigma_{\mu,i}^2 = \left(\frac{5}{\hat{z}_i \ln(10)}\right)^2 \left[\sigma_{z,i}^2 + \frac{\sigma_{\text{pec}}^2}{c^2}\right]. \tag{2}$$

Following Mandel et al. (2009), we set $\sigma_{\text{pec}} = 150\ \text{km s}^{-1}$, the value Mandel et al. (2009) obtained from the local infall flow model of Mould et al. (2000).

To ensure the robustness of the posterior distribution, we vary the choice of prior distribution for the residual intrinsic dispersion, σ_{res}, using InvGamma(0.1,0.1), InvGamma(0.03,0.03), InvGamma(0.003,0.003) and LogUniform(-5, 2); InvGamma(a, b) denotes a random variable whose reciprocal follows a Gamma distribution[1] with mode equal to $\frac{b}{a+1}$. While the posteriors for all other parameters are fairly independent of the choice of prior distribution for σ_{res}, the posterior distribution of σ_{res} is sensitive to this choice. (This is not unexpected given the small number of SNIa in our sample.) Thus, we do not use the posterior distribution of σ_{res} to quantify and compare the residual scatter for different models. Instead, we quantify the residual scatter in the Hubble diagram with the Hubble residual between the observed distance modulus,

$$\hat{\mu}_i(M_0, \mathscr{B}) = \hat{m}_{Bi} - \hat{X}_i^{\ T} \mathscr{B} - M_0, \tag{3}$$

and the model distance modulus, $\mu(\hat{z}, \mathscr{C})$, for SNIa i, that is

$$\Delta\mu_i = \hat{\mu}_i(M_0, \mathscr{B}) - \mu(\hat{z}_i, \mathscr{C}). \tag{4}$$

We emphasize that while $\hat{\mu}_i(M_0, \mathscr{B})$ is a function of the observed data, it also depends on the unknown parameters M_0 and $\mathscr{B}$, which need to be estimated from the data. (In the usual χ^2 approach, such parameters are replaced by their estimated value.) Thus, in a Bayesian analysis, $\hat{\mu}_i(M_0, \mathscr{B})$ itself has a posterior distribution. We then calculate the posterior distribution of the sample standard deviation of the $\Delta\mu_i$, i.e.

$$\sigma_{\Delta\mu} = \sqrt{\frac{1}{n-1}\sum_{i=1}^{n}(\Delta\mu_i - \overline{\Delta\mu})^2}, \tag{5}$$

where $\overline{\Delta\mu} = \frac{1}{n}\sum_{i=1}^{n}\Delta\mu_i$. Because $\hat{\mu}_i(M_0, \mathscr{B})$ is a function of the unknown parameters M_0 and $\mathscr{B}$, $\sigma_{\Delta\mu}$ is also a function of M_0 and $\mathscr{B}$ and itself has a posterior distribution. Thus, we calculate the posterior distribution of $\sigma_{\Delta\mu}$. We find that $\sigma_{\Delta\mu}$ is independent of the prior choice (of σ_{res}) and quantifies the residual scatter in the Hubble diagram well. We use $\sigma_{\Delta\mu}$ to compare the performance of the five choices of covariates enumerated in the five cases mentioned previously.

In order to cross-check our numerical results, we obtain samples from the joint posterior distribution of the parameters of interest using both a Gibbs sampler and a Metropolis–Hastings algorithm,

[1] More specifically: if $X \sim \text{InvGamma}(a, b)$, its probability density is given by $p(x) = \frac{b^a}{\Gamma(a)} x^{-a-1} e^{-b/x}$.

Table 2. Posterior means and 1σ marginal posterior intervals for the regression coefficients and population parameters for the five models considered.

Parameter	Covariates				
	x_1	t_2	x_1 and c	t_2 and c	x_1, t_2 and c
α (mag)	0.139 ± 0.060	–	0.168 ± 0.035	–	0.039 ± 0.069
γ (mag/d)	–	0.037 ± 0.011	–	0.037 ± 0.007	0.029 ± 0.014
β (mag/mag)	–	–	3.238 ± 0.560	2.819 ± 0.493	2.948 ± 0.534
M_0^ϵ (mag)	− 19.428 ± 0.070	− 19.345 ± 0.056	− 19.313 ± 0.045	− 19.231 ± 0.040	− 19.250 ± 0.053

Table 3. Posterior percentiles for the Hubble diagram residual scatter, $\sigma_{\Delta\mu}$, for the five models considered. Also included is the shortest 1σ interval, which extends from the maximum to the 68.3th percentile of the posterior distribution.

Covariates	Percentile					
	5th	25th	50th	75th	95th	1σ interval
x_1	0.281	0.281	0.284	0.290	0.309	0.280–0.287
t_2	0.250	0.251	0.254	0.260	0.279	0.250–0.257
x_1 and c	0.159	0.162	0.167	0.174	0.191	0.159–0.171
t_2 and c	0.148	0.150	0.154	0.161	0.178	0.147–0.159
x_1, t_2 and c	0.145	0.150	0.155	0.164	0.184	0.144–0.161

obtaining identical results up to Monte Carlo noise. (Details on the sampling algorithms can be found in Shariff et al. 2016.) We marginalize out the latent variables (via Monte Carlo for the Gibbs sampler and analytically for the Metropolis–Hastings algorithm) and present marginal posterior distributions for the parameters of interest, including $\sigma_{\Delta\mu}$.

3 RESULTS

Table 2 presents the posterior mean and standard deviation of the regression coefficients, as well as of M_0^ϵ for each of the five cases. When t_2 is used as the sole covariate, the (negative of the) slope of the linear relationship with intrinsic magnitude, γ, shows a 3.4σ deviation from zero. When colour is added as an additional covariate, the significance of the t_2 coefficient increases to $>5\sigma$. When all three covariates are used together, the (absolute) values of both the rebrightening time and the stretch correction slopes reduce, suggesting that (as expected) t_2 and x_1 encode similar standardization information.

Since the posterior distributions of $\sigma_{\Delta\mu}$ are highly skewed, Table 3 reports their 5th, 25th, 50th, 75th, and 95th percentiles, rather than their means and the standard deviations. Also shown are 1σ posterior intervals for each distribution; we choose the shortest 1σ intervals which, in this case, extend from the minimum to the 68th percentile of each distribution. The marginal posterior distributions of $\sigma_{\Delta\mu}$ are displayed in Fig. 1 for all five cases considered. Based on the residual scatter in the Hubble diagram, $\sigma_{\Delta\mu}$, in the absence of colour correction, t_2 alone is a better standardization quantity than stretch: the (shortest) 1σ posterior interval is $\sigma_{\Delta\mu} = \{0.250, 0.257\}$ mag for the former, while it is $\sigma_{\Delta\mu} = \{0.280, 0.287\}$ mag for the latter. This can further be seen in the left-hand panel of Fig. 2. On average, t_2 (red) leads to smaller Hubble residuals than x_1 (blue). However, when the colour correction is added to the regression, NIR rebrightening time and stretch lead to similar

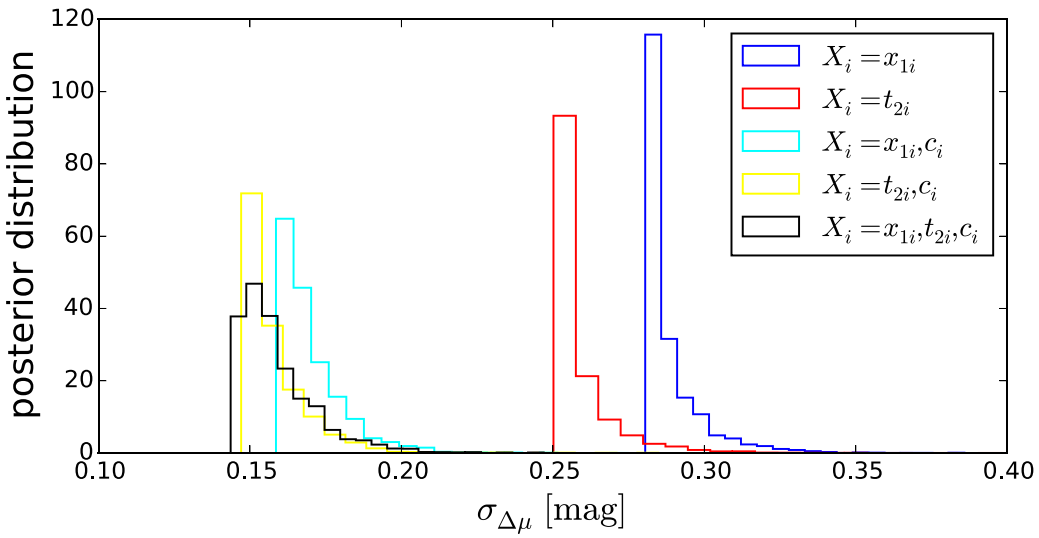

Figure 1. Marginal posterior distributions of the Hubble diagram residual scatter, $\sigma_{\Delta\mu}$, for all the five cases considered. Blue colour is for the case using only the stretch correction, x_1, as standardization covariate, while red is for using only the NIR rebrightening time, t_2. Cyan is for including both stretch and colour, while orange is for using both rebrightening time and colour. Black is for the case when all three covariates are used. Posteriors are normalized.

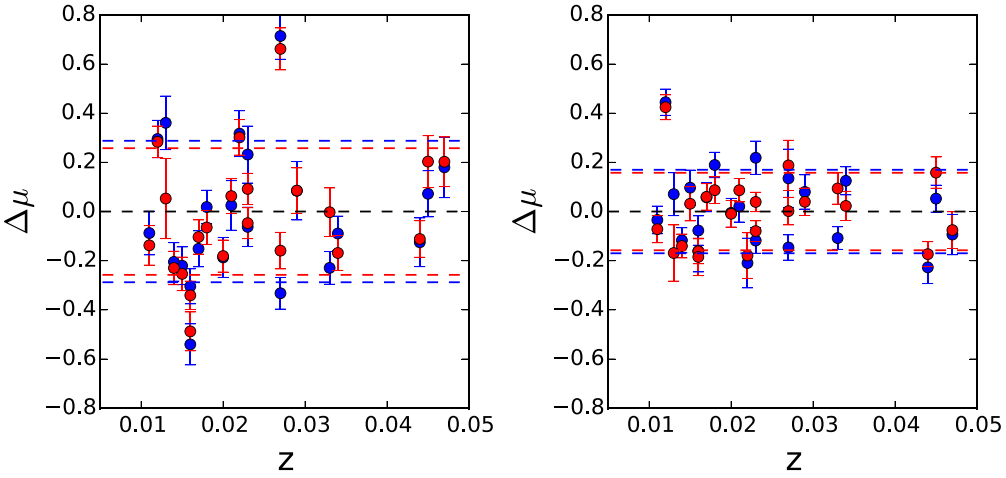

Figure 2. Hubble residuals as a function of redshift. Blue colour is for the cases using the stretch parameter, x_1, as a standardization covariate, while red is for using NIR rebrightening time, t_2, as a covariate. The left-hand (right-hand) panel excludes (includes) colour correction as a covariate. Error bars are the posterior standard deviation of $\Delta\mu$. The dashed red/blue lines indicate the posterior mean of $\sigma_{\Delta\mu}$.

residual scatter, with rebrightening time and colour (1σ posterior interval is $\sigma_{\Delta\mu} = \{0.149, 0.159\}$ mag) performing slightly better than stretch and colour (1σ posterior interval is $\sigma_{\Delta\mu} = \{0.159, 0.171\}$ mag), which is also shown in the right-hand panel of Fig. 2. When using all three covariates together, we observe no further reduction in the residual scatter. We conclude that t_2 can be effectively used as an alternative covariate to x_1 for the standardization of SNIa, but does not lead to further reduction in the residuals scatter in the Hubble diagram once both stretch and colour corrections have been included as covariates. We also consider the case when colour is the only covariate, and find that the posterior distribution of $\sigma_{\Delta\mu}$ is comparable to the case when t_2 is the only covariate.

As shown in Fig. 1, the posterior distributions of $\sigma_{\Delta\mu}$ in all five cases are skewed with long tails for larger values and sharp lower bounds. The sharp lower bound is a feature of the likelihood function, rather than an artefact of the analysis, or a prior-dependent feature. In order to show this, for each of the five cases considered, we compute the maximum likelihood value of $\sigma_{\Delta\mu}$ by optimizing $\{M_0, \mathscr{B}\}$. We find that in all five cases, the maximum likelihood value of $\sigma_{\Delta\mu}$ coincides with the lower bound of its posterior distribution. With a Gaussian likelihood, the maximum likelihood value of the residual variance is formed by minimizing the sum of squared residuals over the possible values of the regression coefficients. This means that there are no values of $\{M_0, \mathscr{B}\}$ that produce values of $\sigma_{\Delta\mu}$ less than the lower bounds in each of the five posterior distributions. As defined in equation (5), $\sigma_{\Delta\mu}$ is a function of M_0 and $\mathscr{B}$ and its posterior distribution is determined by theirs.

4 CONCLUSIONS

We demonstrated on a low-z SNIa sample that the waiting time for NIR rebrightening, t_2, is significantly better at calibrating the peak magnitude of SNIa when compared with stretch alone. Dhawan et al. (2015) found a correlation between t_2, Δm_{15}, and the time of maximum $(B - V)$ colour (denoted by t_L). They inferred that the diversity in t_2 values of SNIa is driven by different masses of ^{56}Ni produced in the explosion. As a follow-up, Dhawan et al. (2016) identified a strong correlation between the peak bolometric luminosity ($L_{\rm max}$) and t_2 for a sample of SNIa with well-measured NIR data. Since the luminosity at peak corresponds to the instantaneous energy deposition rate from ^{56}Ni decay (known as 'Arnett's Rule'; Arnett 1982), the authors used the correlation between $L_{\rm max}$ and t_2 and Arnett's rule to infer a ^{56}Ni mass distribution. The correlation between ^{56}Ni mass and t_2 is stronger than that between ^{56}Ni mass and optical decline rate parameters noted in the literature (e.g. Mazzali et al. 2007; Wang et al. 2008; Scalzo et al. 2014). Therefore, adopting t_2 as a standardization parameter can lead to a smaller residual dispersion because t_2 is more strongly correlated to the physical driver of the luminosity, thus explaining our findings.

Future SN surveys are designed to provide multiband data for a large sample of SNIa. Space-based observatories like *Euclid* and *WFIRST* will be equipped with NIR filters, which will allow us to observe SNIa in the *IYJH* bands out to high-z. With such a configuration, we can expect measurements of t_2 for SNIa at $z > 0.5$, with the view of using this quantity as an alternative standardization parameter to the optical decline rate. Astier et al. (2014) proposed a SN survey with LSST and the *Euclid* satellite out to $z \sim 1.5$. With their survey parameters, they expect a total of ∼700 SNe in the redshift range of $0.75 < z < 1.5$, a sizeable sample to test our standardization procedure at high-z. This would lead to a better understanding of the physical parameters underlying the standardization procedure (e.g. ^{56}Ni mass), to tests of the validity of the empirical stretch correction and to a reduction of the systematic error budget in SNIa cosmology.

ACKNOWLEDGEMENTS

The authors would like to thank Kaisey Mandel for useful comments on an early draft. This work was supported by Grant ST/N000838/1 from the Science and Technology Facilities Council (UK). RT was partially supported by an EPSRC 'Pathways to Impact' grant. DvD was supported by a Wolfson Research Merit Award (WM110023) provided by the British Royal Society and by Marie-Curie Career Integration (FP7-PEOPLE-2012-CIG-321865) grant provided by the European Commission. RT, DvD and HS were supported by a Marie-Skodowska-Curie RISE (H2020-MSCA-RISE-2015-691164) Grant provided by the European Commission.

REFERENCES

Amanullah R., Goobar A., 2011, ApJ, 735, 20
Arnett W. D., 1982, ApJ, 253, 785
Astier P. et al., 2014, A&A, 572, A80

Biscardi I. et al., 2012, A&A, 537, A57
Blondin S., Dessart L., Hillier D. J., 2015, MNRAS, 448, 2766
Contreras C. et al., 2010, AJ, 139, 519
Dhawan S., Leibundgut B., Spyromilio J., Maguire K., 2015, MNRAS, 448, 1345
Dhawan S., Leibundgut B., Spyromilio J., Blondin S., 2016, A&A, 588, A84
Elias J. H., Frogel J. A., Hackwell J. A., Persson S. E., 1981, ApJ, 251, L13
Folatelli G. et al., 2010, AJ, 139, 120
Guy J. et al., 2007, A&A, 466, 11
Hamuy M., Phillips M. M., Suntzeff N. B., Schommer R. A., Maza J., Smith R. C., Lira P., Aviles R., 1996, AJ, 112, 2438
Hook I. M., 2013, Phil. Trans. R. Soc. A, 371, 20282
Kasen D., 2006, ApJ, 649, 939
Kattner S. et al., 2012, PASP, 124, 114
Kim A. G. et al., 2013, ApJ, 766, 84
Krisciunas K., Phillips M. M., Suntzeff N. B., 2004, ApJ, 602, L81
Leibundgut B., 1988, PhD thesis, Univ. Basel
Ma C., Corasaniti P.-S., Bassett B. A., 2016, MNRAS, 463, 1651
Mandel K. S., Wood-Vasey W. M., Friedman A. S., Kirshner R. P., 2009, ApJ, 704, 629
Mandel K. S., Narayan G., Kirshner R. P., 2011, ApJ, 731, 120
March M. C., Trotta R., Berkes P., Starkman G. D., Vaudrevange P. M., 2011, MNRAS, 418, 2308
Mazzali P. A., Röpke F. K., Benetti S., Hillebrandt W., 2007, Science, 315, 825
Mould J. R. et al., 2000, ApJ, 529, 786
Nielsen J. T., Guffanti A., Sarkar S., 2015, preprint (arXiv:1506.01354)
Perlmutter S. et al., 1999, ApJ, 517, 565
Phillips M. M., 1993, ApJ, 413, L105
Rest A. et al., 2014, ApJ, 795, 44
Riess A. G., Press W. H., Kirshner R. P., 1996, ApJ, 473, 588
Riess A. G. et al., 1998, AJ, 116, 1009
Rubin D., Aldering G., Barbary K., Boone K., Chappell G. et al., 2015, ApJ, 813, 137
Scalzo R. et al., 2014, MNRAS, 440, 1498
Shariff H., Jiao X., Trotta R., van Dyk D. A., 2016, ApJ, 827, 1
Stritzinger M. D. et al., 2011, AJ, 142, 156
Tripp R., 1998, A&A, 331, 815
Wang B., Meng X.-C., Wang X.-F., Han Z.-W., 2008, Chin. J. Astron. Astrophys., 8, 71
Wood-Vasey W. M. et al., 2008, ApJ, 689, 377

This paper has been typeset from a TEX/LATEX file prepared by the author.